Sustainable Energy Technologies and Assessments 51 (2022) 101931

Contents lists available at ScienceDirect

Sustainable Energy Technologies and Assessments

journal homepage: www.elsevier.com/locate/seta

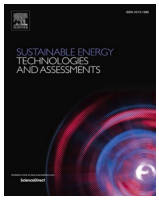

Original article

Very short-term parametric ambient temperature confidence interval forecasting to compute key control parameters for photovoltaic generators

Fermín Rodríguez [a,b,*], Xabier Insausti [b], Gorka Etxezarreta [b], Ainhoa Galarza [a,b], Josep M. Guerrero [c]

[a] Ceit-Basque Research and Technology Alliance (BRTA), Manuel Lardizabal 15, Donostia/San Sebastián 20018, Spain
[b] Universidad de Navarra, Tecnun, Manuel Lardizabal 13, Donostia/San Sebastián 20018, Spain
[c] Center for Research on Microgrids (CROM), Department of Energy Technology, Aalborg University, Aalborg 9220, Denmark

ARTICLE INFO

Keywords:
Confidence interval forecast
Very short-term horizon
Temperature
Smart control
Photovoltaic generation

ABSTRACT

In recent years, various forecasters have been developed to decrease the uncertainty related to the intermittent nature of photovoltaic generation. While the vast majority of these forecasters are usually just focused on deterministic or probabilistic prediction points, few studies have been carried out in relation to prediction intervals. In increasing the reliability of photovoltaic generators, being able to set a confidence level is as important as the forecaster's accuracy. For instance, changes in ambient temperature or solar irradiation produce variations in photovoltaic generators' output power as well as in control parameters such as cell temperature and open voltage circuit. Therefore, the aim of this paper is to develop a new mathematical model to quantify the confidence interval of ambient temperature in the next 10 min. Several error metrics, such as the prediction interval coverage percentage, the Winkler score and the Skill score, are calculated for 95%, 90% and 85% confidence levels to analyse the reliability of the developed model. In all cases, the prediction interval coverage percentage is higher than the selected confidence interval, which means that the estimation model is valid for practical photovoltaic applications.

Introduction

In recent years different eco-friendly technologies such as solar, wave, hydropower, wind and geothermal/biomass have been proposed and developed depending on a countries' renewable resources. However, some of these technologies have been developed more quickly because it is easier to introduce them in the traditional grid, they have higher efficiency or their expected investment return is greater [1,2]. For instance, the installed capacity power of solar, wind and geothermal/biomass technologies has greatly increased in the last decade, and this trend is expected to continue in the following years [3,4]. Traditionally, electric networks were hierarchically organized systems, where generators, transmission and distribution operators and customers had well-defined assignments. However, as the installed capacity as well as the energy generated by solar, wind and geothermal/biomass technologies increases, traditional grid operators have more trouble ensuring system reliability due to the uncertainty introduced by intermittent renewable generation [5].

To be able to guarantee reliable operation of each electric system, network operators need to know what the system's energy demand and the generators' power production will be in different horizon times [6,7,8]. Moreover, some international bodies, such as the European Commission or the International Renewable Energy Agency, are creating roadmaps that will allow renewable technologies to both produce electric power and provide ancillary services in the near future as a means to maximizing energy production [9,10].

To achieve the goal of making eco-friendly generators more reliable to provide both, electric power and ancillary services, researchers have developed different prediction horizon forecasters. Based on the horizon step, these tools are commonly divided in the following groups [6]: a) very short-term forecasters which provides information for the next minutes and are commonly used for real-time dispatch operations [11,12], b) short-term forecasters that provides information for the range from a few minutes to a few hours, and forecast values are applied at unit commitment/economic dispatch operations [13,14] and c) medium-term and long-term forecasters which makes forecasts for the

* Corresponding author at: Ceit-Basque Research and Technology Alliance (BRTA), Manuel Lardizabal 15, Donostia/San Sebastián 20018, Spain.
E-mail address: frlalanne@ceit.es (F. Rodríguez).

https://doi.org/10.1016/j.seta.2021.101931
Received 25 February 2021; Received in revised form 27 June 2021; Accepted 20 December 2021
Available online 31 December 2021

ranges of a day to few weeks ahead and few weeks to months ahead. The information provided is used for maintenance and new infrastructure planning [15,16].

From [17,18,19], it can be deduced that it is mandatory to improve the control strategies of renewables by developing accurate forecasters in all the above-mentioned horizons. These control strategies would allow renewables to raise their installed power capacity to provide power and also to make them suitable for ancillary service operations. With regards to ancillary services, accurate very short-term prediction tools with time steps lower than 15 min ahead must be developed [17]. Although different renewable technologies have been developed in recent years, solar and wind technologies seems to be the most suitable ones to provide ancillary services.

With regard to photovoltaic (PV) generators, Ayvazoğluyüksel et al. [20] established solar irradiation, PV cell temperature (TC), PV efficiency, and generated output power (PM) as relevant parameters for improving generators' control strategies. However, a close analysis of Ayvazoğluyüksel et al.'s study [20], shows that TC is also affected by ambient temperature and wind speed [21,22]. Moreover, it was also demonstrated in [23] that other less relevant control parameters such as open voltage circuit (VOC) and short circuit current (ISC) are also affected by TC and therefore, by ambient temperature and wind speed. Consequently, we determined that solar irradiation, wind speed and ambient temperature are the involved meteorological parameters in PV generation. Solar irradiation [24,25] and wind speed [26,17] parameters very short-term forecasting has been deeply examined due to their strong relationship with PV and wind power generation. However, ambient temperature, has been typically predicted in order to develop management algorithms or load demand forecasting tools [28,29], but few forecasters that predict this parameter have been developed in relation to PV generation.

Conventionally, very short-term prediction tools have been organized into two main groups: statistical or physical approaches [30]. While statistical approaches use a combination of historical databases and machine learning tools to develop forecasters [24–27], physical approaches are based on the mathematical expression of weather or sky imagery via satellites [31,32]. However, these last types of approaches are less developed due to the high cost or lack of the required equipment. With respect to statistical approaches, the vast majority of the studies have focused on increasing the accuracy of deterministic point forecasters (DPFs). Although Artificial Neural Networks (ANNs) are the most popular statistical approaches for forecasting different parameters [12,24,33], other researchers have based their forecasters on other statistical approaches like support vector machines [34] or autoregressive approaches [35,36]. Nevertheless, some authors have recently claimed that DPFs do not provide complete information due to their deviation between real and forecasted values [37,38], and thus they have suggested that confidence interval forecasters (CIFs) be developed to improve the quality of the information. In addition, these CIFs also allowed decision makers avoiding local minima in their optimization algorithms as well as an over cost of the system when they are quantifying the power reserve [39].

Based on approaches developed in recent years for DPFs, CIFs provide additional information which can help grid operators or energy management systems to make better decisions in scheduling as well as ensure power systems' real-time stability. CIFs can be classified into two main groups: parametric approaches, which are based on developing forecasters through probability density functions (PDFs), or non-parametric approaches, which do not rely on using PDFs. With regard to parametric approaches, after reviewing the literature, we found some studies where different PDFs, such as Normal, Laplacian or Gaussian distributions, were used to predict random variables [40,41]. For instance, Junior et al. [41] described PV generation errors by either Laplacian or Gaussian PDFs; the related parameters for each PDF were calculated from a one-year database, where the deviation between measured and forecasted data was recorded; then, the CIF was computed using calculated PDFs.

However, other studies do not consider using PDFs to develop CIFs [38,42]. Some of the most popular non-parametric approaches are: quantile regression approaches, which are based on obtaining a relationship between a previously analysed group of relevant parameters and the target parameter's chosen quantile [43]; the bootstrap method, which relies on using the chosen samples' distribution instead of the population's distribution [37,44], has been also widely applied in modelling non-parametric PDFs.

This study develops a novel parametric model for very short-term ambient temperature CIF, namely for the next 10 min. The model relies on examining the effect that produces a small variation in each parameter of the forecaster in the final predicted value. Our model is based on function linearization. Main contributions of this study are:

1) A novel very short-term parametric ambient temperature CIF, for 10 min ahead, was examined. The parametric approach is based on the combination of a feedforward neural network, the optimal number of nearest meteorological stations, and the effect of each parameter of the forecaster in the final predicted value through the use of partial derivatives. CIF accuracy was validated with the database for a specific location, Vitoria-Gasteiz, Basque Country.
2) The same mathematical model for CIF prediction was applied in two different DPF approaches: a single station model and a spatiotemporal or multiple station model. Computed error metrics show that the spatiotemporal model overcomes the single station approach when confidence intervals are predicted.
3) Our model's reliability was examined through an analysis of the accuracy of predicted values for different confidence levels, namely 95%, 90% and 85%. For each of those confidence levels, different accuracy and sharpness error metrics were calculated to examine the reliability of the proposed forecaster.

Methodology

To develop our model, we used as baseline a couple of temperature statistical approach forecasters that were developed in a previous work [45]. Table 1 summarizes the main characteristics of those forecasters, which are based on feedforward ANNs. The feedforward neural network (FFNN) forecaster only uses target location information to predict future temperature values, whereas the spatiotemporal feedforward neural network (FFNNST) forecaster uses information from the target location

Table 1
Main characteristics of statistical approach forecasters for CIFs development.

Network type	FFNN	FFNNST
Inputs (K)	146 = season (1), time (1), target location's temperature data (144)	1022 = season (1), time (1), target location's (144) and surroundings stations' temperature data (876)
Outputs	1 – temperature	1 – temperature
Number of Layers	3 – input, hidden, output	3 – input, hidden, output
Number of Hidden Neurons (N)	15	15
Number of Weights	2190	15,330
Number of Biases	15	15

as well as from the optimized number of surrounding stations to predict future values. More information about FFNN as well as FFNNST, and how they work can be found in [45].

In the context of this paper, the output of the n-th neuron of the hidden layer is represented by a real function f of a linear combination of several variables that is mathematically expressed as:

$$z_n = f\left(\sum_{k=1}^{K} w_{k,n}[x]_{k,1} + b_n\right), n \in \{1, 2, \cdots, N\} \tag{1}$$

where $x \in \mathbb{R}^K$ is the input, $w_{k,n}$ are the weights of the n-th neuron with $k \in \{1, 2, \cdots, K\}$, b_n is the bias value of the n-th neuron and

$$f(\omega) = \frac{1}{1 + e^{-\omega}}. \tag{2}$$

Similarly, the output neuron is represented by a linear combination of the outputs of the hidden neurons:

$$\widehat{y} = \sum_{n=1}^{N} w_{n,N+1} z_n + b_{N+1}. \tag{3}$$

The CIF model that we develop in this study is based on analysing the actual effect that produces a small variation of each neuron's weights and biases in the forecaster's final output. By estimating these variations, the desired confidence interval is predicted.

Confidence interval forecast model

In this subsection we obtain the CIF model. For the reader's convenience, Fig. 1 summarizes the steps followed in this subsection.

We denote with $\varphi = \left(w_{1,1}, \cdots, w_{K,1}, b_1, \cdots, w_{1,N}, \cdots, w_{K,N}, b_N, w_{1,N+1}, \cdots, w_{N,N+1}, b_{N+1}\right) \in \mathbb{R}^{N(K+2)+1}$ the column vector of all weights and biases of the neurons that compose the ANN. The output of the ANN can be represented as $g(x;\varphi)$, where $x \in \mathbb{R}^K$ is the input and g is the scalar function that represents the ANN, i.e.,

$$g(x;\varphi) = \sum_{n=1}^{N} w_{n,N+1} f\left(\sum_{k=1}^{K} w_{k,n}[x]_{k,1} + b_n\right) + b_{N+1}. \tag{4}$$

Observe that for a fixed ANN, the current output only depends on the current input and on the set of parameters φ.

Consider a physical system whose output y can be modelled by an unknown scalar function h as

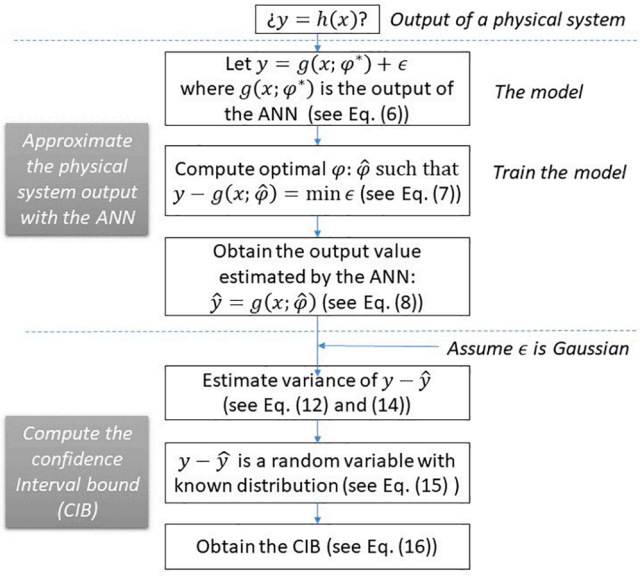

Fig. 1. Flowchart of the most relevant steps to compute proposed CIF model.

$$y = h(x). \tag{5}$$

The goal is to approximate the physical system's output with the ANN, in such a way that

$$y = g(x;\varphi^*) + \epsilon \tag{6}$$

where ϵ is the approximation error and $\varphi^* \in \mathbb{R}^{N(K+2)+1}$ is the optimal set of parameters, which is unknown. Assume that L input/output pairs of the physical system are known, namely $(x_1, y_1), \cdots, (x_L, y_L)$. Let $\widehat{\varphi} = \left(\widehat{\varphi}_1, \cdots, \widehat{\varphi}_{N(K+2)+1}\right)^T \in \mathbb{R}^{N(K+2)+1}$ denote the set of parameters that minimize the approximation errors in the mean square sense, that is,

$$\widehat{\varphi} = \underset{\varphi \in \mathbb{R}^{N(K+2)+1}}{\operatorname{argmin}} \sum_{t=1}^{L} \left(y_t - g(x_t;\varphi)\right)^2. \tag{7}$$

In other words, $\widehat{\varphi}$ is the least squares estimator of φ^*. The least squares problem (7) can be efficiently solved using the well-known Levenberg–Marquardt algorithm [46]. Consequently, we denote with $\widehat{y}$ the output value estimated by the ANN, that is,

$$\widehat{y} = g(x;\widehat{\varphi}). \tag{8}$$

From (6) and (8), and using a first-order Taylor polynomial, the approximation error can be written as

$$\begin{aligned} \epsilon &= y - g(x;\varphi^*) \approx y - g(x;\widehat{\varphi}) - \left(D(\widehat{\varphi})\right)^{\mathrm{T}}(\varphi^* - \widehat{\varphi}) \\ &= y - \widehat{y} - (\varphi^* - \widehat{\varphi})^{\mathrm{T}} D(\widehat{\varphi}) \end{aligned} \tag{9}$$

where $D(\widehat{\varphi})$ is the gradient of g evaluated at $\varphi = \widehat{\varphi}$, that is,

$$D(\widehat{\varphi}) = \left(\frac{\partial g(x;\widehat{\varphi})}{\partial \widehat{\varphi}_1}, \cdots, \frac{\partial g(x;\widehat{\varphi})}{\partial \widehat{\varphi}_{N(K+2)+1}}\right)^T. \tag{10}$$

Observe that (9) can be written as

$$y - \widehat{y} = \epsilon - (\widehat{\varphi} - \varphi^*)^{\mathrm{T}} D(\widehat{\varphi}). \tag{11}$$

In order to compute the sought confidence interval bound (CIB), we perform a statistical analysis and we view y and $\widehat{y}$ as random variables. We assume that the approximation error ϵ is a Gaussian random variable with zero mean and variance σ^2 and independent from $(\widehat{\varphi} - \varphi^*)$. Observe that under this assumption, for $N(K+2) + 1 \leq M \leq L$

$$s^2 = \frac{1}{M - N(K+2) - 1} \sum_{t=1}^{M} \left(y_t - g(x_t;\widehat{\varphi})\right)^2 \tag{12}$$

is the unbiased estimator of σ^2 and,

$$E\left[(\widehat{\varphi} - \varphi^*)^T (\widehat{\varphi} - \varphi^*)\right] = \sigma^2 C^{-1}, \tag{12}$$

Where E denotes expectation, $C = \left(\mathrm{J}(\widehat{\varphi})\right)^T \mathrm{J}(\widehat{\varphi})$, and $\mathrm{J}(\widehat{\varphi})$ is the Jacobian matrix

$$\mathrm{J}(\widehat{\varphi}) = \begin{bmatrix} \frac{\partial g(x_1,\widehat{\varphi})}{\partial \widehat{\varphi}_1} & \cdots & \frac{\partial g(x_1,\widehat{\varphi})}{\partial \widehat{\varphi}_{N(K+2)+1}} \\ \vdots & \ddots & \vdots \\ \frac{\partial g(x_M,\widehat{\varphi})}{\partial \widehat{\varphi}_1} & \cdots & \frac{\partial g(x_M,\widehat{\varphi})}{\partial \widehat{\varphi}_{N(K+2)+1}} \end{bmatrix}. \tag{13}$$

Therefore, from (11) and (13) we conclude that

$$\begin{aligned} E\left[(y - \widehat{y})^2\right] &= E\left[\epsilon^2\right] + \left(D(\widehat{\varphi})\right)^T E\left[(\widehat{\varphi} - \varphi^*)(\widehat{\varphi} - \varphi^*)^T\right] D(\widehat{\varphi}) \\ &= \sigma^2\left(1 + \left(D(\widehat{\varphi})\right)^T C^{-1} D(\widehat{\varphi})\right). \end{aligned} \tag{14}$$

Finally, for a large enough M samples taken from the training database,

$$T = \frac{y - \widehat{y}}{s\sqrt{1 + \left(D(\widehat{\varphi})\right)^T C^{-1} D(\widehat{\varphi})}} \tag{15}$$

is a random variable with Student's t-distribution and $M-N(K+2)-1$ degrees of freedom [47]. Therefore, an approximated CIB for the estimated output $\hat{y}$ with confidence $100(1-\alpha)\%$ is given by

$$\mathrm{CIB} = \hat{y} \pm t^{\alpha/2}_{M-N(K+2)-1} s\sqrt{1+(D(\hat{\varphi}))^T C^{-1} D(\hat{\varphi})}, \tag{16}$$

where $\alpha \in (0,1)$, $t^{\alpha/2}_{M-N(K+2)-1} = P\left(T < \frac{\alpha}{2}\right)$ and P denotes probability.

Uncertainty evaluation error metrics

From previous works in the literature (see, e.g., [38,40,48]), error metrics can be classified into two main groups: the first group focuses on analysing forecasters' reliability through indexes such as prediction interval coverage percentage (PICP) or coverage error (CE), and the second group examines sharpness, which is related to how close upper and lower bounds are from the forecasted point through a skill score (SS) or confidence interval normalized average width (CINAW) indexes. In this section, we compute five error metrics.

From (16), the actual output of the physical system at time instance t, y_t, is expected to lie within the CIB, that is, $y_t \in (\mathrm{LB}_\alpha(x_t), \mathrm{UB}_\alpha(x_t))$, where

$$\mathrm{LB}_\alpha(x_t) = g(x_t;\hat{\varphi}) - t^{\frac{\alpha}{2}}_{M-N(K+2)-1} s\sqrt{1+(D(\hat{\varphi}))^T C^{-1} D(\hat{\varphi})}, \tag{17}$$

$$\mathrm{UB}_\alpha(x_t) = g(x_t;\hat{\varphi}) + t^{\frac{\alpha}{2}}_{M-N(K+2)-1} s\sqrt{1+(D(\hat{\varphi}))^T C^{-1} D(\hat{\varphi})}. \tag{18}$$

The best known uncertainty error metric for analysing a CIF's reliability is the PICP index. PICP examines the difference between the actual values that fall into CIBs and those that do not. The larger the PICP is, the better the CIF's reliability. PICP can be mathematically expressed as,

$$\mathrm{PICP}_\alpha = \frac{1}{T}\sum_{t=1}^{T} \chi_{(\mathrm{LB}_\alpha(x_t),\mathrm{UB}_\alpha(x_t))}(y_t) \tag{19}$$

where T is the total amount of tested points, and χ_S denotes the characteristic (or indicator) function of $S \subseteq \mathbb{R}$, that is,

$$\chi_S(\omega) = \begin{cases} 1 & \text{if } \omega \in S, \\ 0 & \text{otherwise.} \end{cases} \tag{20}$$

If the PICP value is greater than or equal to the user's selected confidence level (i.e., $\mathrm{PICP}_\alpha \geq (1-\alpha)$), then the CIF model is valid; otherwise, the model needs to be revised in order to increase its reliability [38]. In addition, the width of the interval obtained through the examined CIF is also a key parameter that must be analysed. It must be taken into account that a narrower prediction interval, one that is closer to the actual value, is identified with a better and more accurate CIF. This concept is also known in the literature as sharpness [40,48]. The confidence interval's width (CIW) can be defined as,

$$\mathrm{CIW}_\alpha(x_t) = \mathrm{UB}_\alpha(x_t) - \mathrm{LB}_\alpha(x_t) \tag{21}$$

In 1972, Winkler [49] defined the so called winkler score (WS), which is used to analyse the forecasted intervals' quality and sharpness. Winkler defined the score as

$$\mathrm{WS}_\alpha(x_t) = \begin{cases} -2\alpha\mathrm{CIW}_\alpha(x_t) - 4(\mathrm{LB}_\alpha(x_t) - y_t) & \text{if } y_t \leq \mathrm{LB}_\alpha(x_t), \\ -2\alpha\mathrm{CIW}_\alpha(x_t) & \text{if } \mathrm{LB}_\alpha(x_t) < y_t < \mathrm{UB}_\alpha(x_t), \\ -2\alpha\mathrm{CIW}_\alpha(x_t) - 4(y_t - \mathrm{UB}_\alpha(x_t)) & \text{if } y_t \geq \mathrm{UB}_\alpha(x_t). \end{cases} \tag{22}$$

The overall score, $\overline{\mathrm{WS}_\alpha}$, can be computed as,

$$\overline{\mathrm{WS}_\alpha} = \frac{1}{T}\sum_{t=1}^{T} \mathrm{WS}_\alpha(x_t). \tag{23}$$

As shown in (23), when the actual value y_t falls into the CIB, the WS penalty just depends on the interval's width, whereas when y_t falls out from the bounds, the WS penalization is larger and does not depend only on the interval's width. Moreover, $\overline{\mathrm{WS}_\alpha}$ is usually normalized by an appropriate parameter P:

$$\overline{\mathrm{WSN}_\alpha} = \frac{1}{P}\overline{\mathrm{WS}_\alpha}. \tag{24}$$

The less negative the WS is, the better the sharpness of the CIF. The CINAW is an easy way of analysing and computing the quality of the forecasted confidence intervals and is expressed as,

$$\mathrm{CINAW}_\alpha = \frac{1}{TP}\sum_{t=1}^{T} \mathrm{CIW}_\alpha(x_t). \tag{25}$$

The closer to zero the CINAW parameter is, the sharper and narrower the CIBs calculated by the CIF. The last computed sharpness index is denoted as the SS and it is defined as,

$$\mathrm{SS}_\alpha = \frac{1}{T}\sum_{t=1}^{T} \left|\chi_{(\mathrm{LB}_\alpha(x_t),\mathrm{UB}_\alpha(x_t))}(y_t) - (1-\alpha)\right| max(|\mathrm{LB}_\alpha(x_t) - y_t|, |y_t - \mathrm{UB}_\alpha(x_t)|) \tag{26}$$

The SS index is always positive and a lower value means higher scores. As happens with the WS index, the SS index is also often normalized by an appropriate parameter P:

$$\mathrm{SSN}_\alpha = \frac{1}{P}\mathrm{SS}_\alpha. \tag{27}$$

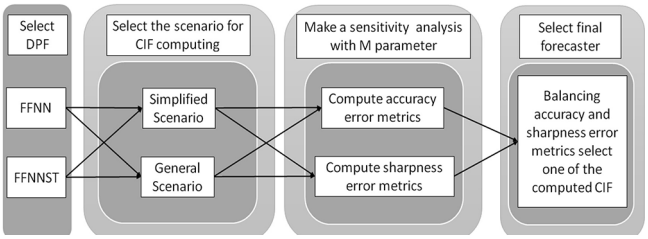

Fig. 2. Flowchart of the most relevant decisions take to select final CIF's configuration.

Results and discussion

Description of the data used

The meteorological information stored in the database was provided by Euskalmet, the Basque Government's Meteorological Agency (http://www.euskalmet.euskadi.eus/). While the database used in FFNN only contains the target station's ('C040 Vitoria-Gasteiz') temperature information with 10 min resolution, the database used in FFNNST contains the target station's information as well as the surrounding stations' information with the same temporal resolution. For the development of FFNN and FFNNST, data from the years 2015–16 were used in the training step, whereas data from 2017 were used in the validation step to obtain the estimated $\hat{y}$ values (see Eq. (8)). In this study, it was also necessary to differentiate between both databases; while the 2015–16 database was used to fit $\mathrm{J}(\hat{\varphi})$, the 2017 database was used to compute $D(\hat{\varphi})$.

As demonstrated in several studies [50–53], databases of DPFs are normalized to increase the generalization capacity of forecasters and thus improve the accuracy of predictions from previously unseen data. Therefore, in this study both the training and validation databases were normalized to have zero mean and unit variance. In addition, the databases use had to be checked to examine if there were corrupt data, such as abnormal or missing values. Ouyang et al. [54] suggested using exponential smoothing equations for abnormal values, whereas linear or spline interpolation is used when there are missing data. These strategies were applied in this study. Fig. 2, shows a flowchart that explains the

Table 2
$PICP_{0.05}$ results to fit M parameter for both scenarios (FFNN model).

	Scenario	M	Date			
			09/02/2017	04/05/2017	25/07/2017	16/08/2017
$100 \times PICP_{0.05}$ (T = 144)	Simplified	21	91.67	93.06	93.06	97.22
		20	98.61	99.31	99.31	100.00
		19	98.61	99.31	99.31	100.00
		18	100.00	100.00	100.00	100.00
	General	2285	95.13	99.31	95.83	96.52
		2278	97.91	99.31	96.52	97.91
		2272	98.61	99.31	96.53	97.92
		2260	98.61	100.00	99.31	100.00

main decisions taken in the following sections.

Results of CIF for FFNN forecaster

In order to develop the CIF's structure, we considered two scenarios:

a) Simplified scenario: we assumed that the output of the ANN mostly depends on the $N+1 = 16$ parameters of the last layer's neuron (i.e., $w_{1,N+1}$, $\cdots$, $w_{N,N+1}$, b_{N+1}). Accordingly, we set $\frac{\partial g(x_t,\widehat{\varphi})}{\partial \widehat{\varphi}_j} = 0$ for $j \in \{1, 2, \cdots, N(K+1)\}$ and $t \in \{1, 2, \cdots, M\}$.
b) General scenario: we considered all the $N(K+2)+1 = 2221$ parameters of the ANN.

The PICP results for randomly chosen days obtained from these sensitivity analyses with a confidence level $CL = 100(1-\alpha) = 95\%$ are presented in Table 2 for both scenarios.

From Table 2, we conclude that the lower the number of samples is, the better the accuracy of the CIF. This fact is related to the approach's ability to generalize, i.e., the ability to produce accurate predictions with previously unseen data. Therefore, if databases with a large number of samples are used, the proposed approach memorizes instead of learns and its accuracy reduces. From the mathematical analysis performed in Section 2, recall that the number of samples M is conditioned by $N(K+2) + 1 \leq M \leq L$.

In addition, the forecasters obtained for both scenarios are valid because they satisfy the condition $PICP_\alpha > (1-\alpha)$ for at least one of the chosen data sets, so it will be necessary to examine the sharpness error metrics. In those indexes where a normalization parameter P is required for computation, P takes the average temperature value for the year for the target location, Vitoria-Gasteiz, Basque Country, which is 12 °C. Table 3 shows the results for each computed sharpness error metric in those cases where $PICP_\alpha > (1-\alpha)$.

In terms of the simplified scenario, the results suggest that the lower the number of samples, the higher the associated PICP error metrics. However, if the sharpness error metrics are examined, a higher PICP is based on a wider range of the forecasted interval. Therefore, depending on the application, the user of the forecaster must decide whether a higher PICP or a narrower interval is preferable, balancing both error metrics. In this study, a database with $M = 20$ samples was chosen as the optimal forecaster to compare with other computed forecasters. With regard to the general scenario, we obtained the same conclusions as for the simplified scenario; for this scenario, a database with $M = 2278$ samples was chosen in order to balance accuracy and sharpness error metrics.

To compare the forecasters for both scenarios and decide which has better skills, it was necessary to compare samples that had similar PICP values. Indeed, in comparing the sharpness error metrics for the same PICP values, it was observed that the forecaster obtained from the general scenario outperforms the forecaster obtained from the simplified scenario and obtains narrower interval predictions.

Results of CIF for FFNNST forecaster

With respect to the FFNNST forecaster's parameter fitting, we again consider the simplified and the general scenario. In this case, the simplified scenario considers $N+1 = 16$ relevant parameters while the general scenario considers all the $N(K+2)+1 = 15361$ parameters. The PICP results from these sensitivity analyses with a confidence level $CL = 100(1-\alpha) = 95\%$ are presented in Table 4 for both scenarios.

As occurred with the FFNN CIF, the lower the number of samples, the higher the PICP of the CIF. The forecasters obtained for both scenarios were valid because they satisfied the condition $PICP_\alpha > (1-\alpha)$ for at least one of the chosen data sets, and thus it was necessary to examine

Table 4
$PICP_{0.05}$ results to fit M parameter for both scenarios (FFNNST model).

	Scenario	M	Date			
			09/02/2017	04/05/2017	25/07/2017	16/08/2017
$100 \times PICP_{0.05}$ (T = 144)	Simplified	21	84.02	93.75	94.44	91.66
		20	91.67	93.75	90.97	95.83
		19	95.83	95.83	95.83	98.61
		18	97.92	97.92	97.92	98.61
	General	15,747	14.59	22.92	21.53	23.61
		15,438	55.56	74.30	66.67	62.50
		15,387	96.53	99.31	96.53	97.92
		15,374	100.00	100.00	100.00	100.00

Table 3
Error metrics for M fitting sets for both scenarios (FFNN model).

	Date	Simplified scenario			General scenario			
		20	19	18	2285	2278	2272	2260
$100 \times PICP_{0.05}$ (T = 144)	09/02/2017	98.61	98.61	100.00	95.13	97.91	98.61	98.61
	04/05/2017	99.31	99.31	100.00	99.31	99.31	99.31	100.00
	25/07/2017	99.31	99.31	100.00	95.83	96.52	96.53	99.31
	16/08/2017	100.00	100.00	100.00	96.52	97.91	97.92	100.00
$100 \times \overline{WSN_{0.05}}$ (T = 144)	09/02/2017	−1.55	−1.57	−3.05	−1.13	−1.13	−1.15	−1.51
	04/05/2017	−1.64	−2.15	−3.74	−1.36	−1.45	−1.57	−2.20
	25/07/2017	−1.39	−1.68	−3.06	−1.01	−1.01	−1.06	−1.33
	16/08/2017	−1.49	−1.86	−2.74	−0.83	−0.83	−0.93	−1.22
$100 \times CINAW_{0.05}$ (T = 144)	09/02/2017	14.39	14.78	30.51	8.78	9.21	10.31	14.85
	04/05/2017	16.30	21.24	37.49	12.85	13.78	14.90	21.95
	25/07/2017	13.72	16.75	30.62	7.65	8.15	8.98	12.80
	16/08/2017	14.92	18.62	27.43	6.98	7.39	8.22	12.20
$100 \times SSN_{0.05}$ (T = 144)	09/02/2017	0.46	0.46	0.84	0.33	0.35	0.35	0.44
	04/05/2017	0.48	0.60	1.00	0.40	0.43	0.46	0.62
	25/07/2017	0.40	0.47	0.82	0.29	0.29	0.31	0.39
	16/08/2017	0.43	0.52	0.74	0.25	0.25	0.28	0.36

Table 5
Error metrics for M fitting sets for both scenarios (FFNNST model).

	Date	Simplified scenario		General scenario	
		19	18	15,387	15,374
$100 \times PICP_{0.05}$ (T = 144)	09/02/2017	95.83	97.92	96.53	100.00
	04/05/2017	95.83	99.31	99.31	100.00
	25/07/2017	95.83	97.92	96.53	100.00
	16/08/2017	98.61	98.61	97.92	100.00
$100\times\overline{WSN_{0.05}}$ (T = 144)	09/02/2017	−1.40	−1.95	−1.23	−2.02
	04/05/2017	−1.21	−1.73	−1.13	−2.49
	25/07/2017	−0.97	−1.39	−0.96	−1.64
	16/08/2017	−0.84	−1.29	−0.84	−1.59
$100 \times CINAW_{0.05}$ (T = 144)	09/02/2017	9.88	18.22	9.66	20.23
	04/05/2017	9.72	17.16	11.24	24.86
	25/07/2017	7.53	13.11	7.38	16.44
	16/08/2017	7.89	12.86	7.43	15.89
$100\times SSN_{0.05}$ (T = 144)	09/02/2017	0.40	0.54	0.36	0.58
	04/05/2017	0.35	0.50	0.35	0.69
	25/07/2017	0.28	0.39	0.28	0.47
	16/08/2017	0.26	0.37	0.26	0.45

the sharpness error metrics again. As was done for the FFNN forecaster,P took the average temperature value during the year for the target location, Vitoria-Gasteiz, Basque Country, which was 12 °C. Table 5 shows the results for each computed sharpness error metric in those cases where $PICP_\alpha > (1-\alpha)$.

Based on the criteria of balancing the accuracy and interval width of the forecasters obtained in both scenarios, for the simplified scenario we chose the database with $M = 19$ samples, whereas for the general scenario we chose the database with $M = 15387$ samples. From the results presented in Table 9, it can be seen that the forecaster obtained from the general scenario outperforms the forecaster obtained from the simplified scenario, due to the fact that in the vast majority of the cases for narrower sharpness error metrics the PICP is higher.

Optimal CIF choice

Table 6 summarizes the error metrics for the chosen FFNN and FFNNST forecasters.

To be able to properly analyse the results provided in Table 6, it is necessary to classify the data sets in different cases:

- Case 1: FFNN and FFNNST have the same or similar PICP values. Six of the ten chosen data sets are in this situation (04/05, 14/06, 25/07, 15/08, 16/08, 28/09). In five of those six tested data sets, the FFNNST forecaster produced more accurate predictions while achieving a narrower interval for the same or similar PICP value.
- Case 2: FFNN and FFNNST have the same or similar sharpness error metric values. Three out of ten examined data sets are in this situation (05/03, 10/11, 17/12). In all these cases, the FFNNST forecaster produced more accurate predictions as it had higher PICP values for the same or similar sharpness error metrics.
- Case 3: Higher PICP value for narrower sharpness error metric values. One of the analysed data sets is in this situation (09/02). The FFNN forecaster achieved a higher PICP value with a narrower interval.

Table 6
Error metrics for the chosen FFNN and FFNNST forecasters for.CL = 95%

Date	$100 \times PICP_{0.05}$ (T = 144)		$100\times\overline{WSN_{0.05}}$ (T = 144)		$100 \times CINAW_{0.05}$ (T = 144)		$100\times SSN_{0.05}$ (T = 144)	
	FFNN	FFNNST	FFNN	FFNNST	FFNN	FFNNST	FFNN	FFNNST
04/05/2017	99.31	99.31	−1.57	−1.13	14.90	11.24	0.46	0.35
14/06/2017	100.00	99.31	−2.84	−1.80	28.42	17.76	0.80	0.54
25/07/2017	96.53	96.53	−1.06	−0.96	8.98	7.38	0.31	0.28
15/08/2017	100.00	100.00	−2.13	−2.01	23.11	20.11	0.64	0.57
16/08/2017	97.92	97.92	−0.93	−0.84	8.22	7.43	0.28	0.26
28/09/2017	100.00	100.00	−1.84	−2.30	18.44	23.03	0.53	0.66
05/03/2017	97.92	98.61	−1.13	−1.13	10.65	10.53	0.32	0.32
10/11/2017	97.92	98.61	−0.60	−0.62	5.63	6.01	0.19	0.19
17/12/2017	95.83	97.92	−0.87	−0.87	6.73	6.95	0.26	0.26
09/02/2017	97.91	96.53	−1.15	−1.23	10.31	9.66	0.35	0.36

Table 7
Calculated error metrics by FFNNST CIF for CL = 90% and.CL = 85%

Date	$100 \times PICP_\alpha$ (T = 144)		$100\times\overline{WSN_\alpha}$ (T = 144)		$100 \times CINAW_\alpha$ (T = 144)		$100\times SSN_\alpha$ (T = 144)	
	α = 0.1	α = 0.15	α = 0.1	α = 0.15	α = 0.1	α = 0.15	α = 0.1	α = 0.15
04/05/2017	97.92	95.14	−1.93	−2.63	9.33	8.26	0.60	0.79
14/06/2017	99.31	98.61	−3.02	−4.03	14.74	13.05	0.93	1.26
25/07/2017	93.06	91.67	−1.57	−2.08	6.12	5.43	0.45	0.59
15/08/2017	100.00	99.31	−3.34	−4.44	16.69	14.78	0.97	1.30
16/08/2017	92.36	90.97	−1.42	−1.93	6.16	5.46	0.42	0.57
28/09/2017	100.00	100.00	−3.82	−5.08	19.11	16.92	1.13	1.53
05/03/2017	97.92	97.22	−1.87	−2.48	8.74	7.74	0.54	0.72
10/11/2017	97.92	97.22	−1.03	−1.38	4.99	4.41	0.33	0.45
17/12/2017	94.44	90.97	−1.39	−1.86	5.77	61.30	0.41	0.54
09/02/2017	94.44	95.14	−2.00	−2.63	8.01	8.26	0.59	0.79

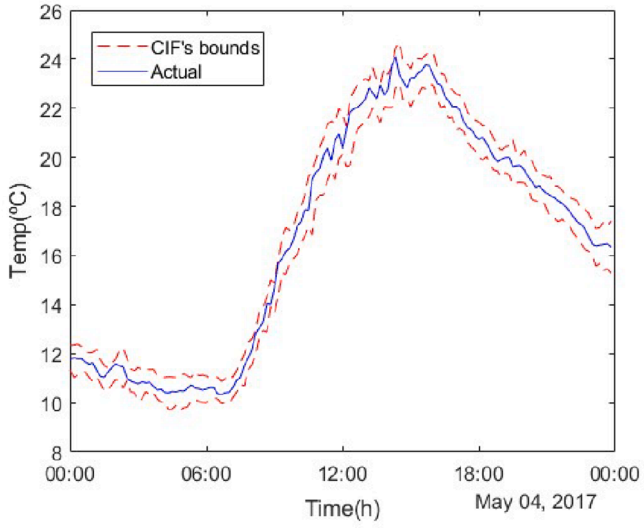

Fig. 3. CIF and actual temperature evolution for May 4, 2017.

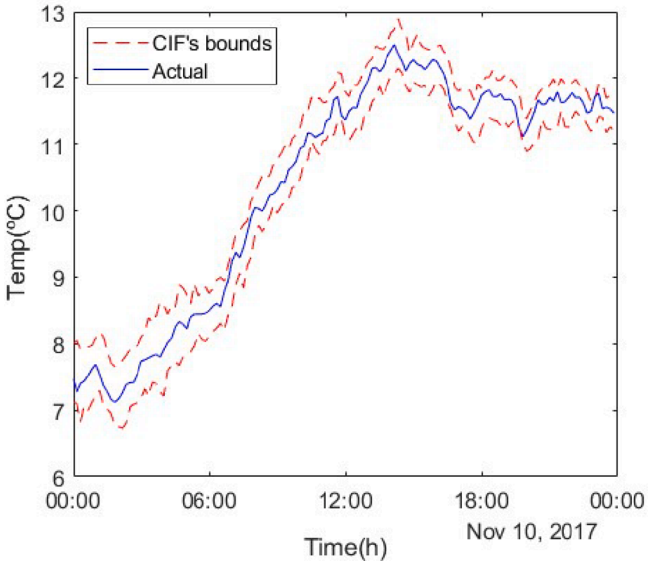

Fig. 4. CIF and actual temperature evolution for November 11, 2017.

Based on this comparison of the predictions provided by each forecaster, we concluded that FFNNST CIF was more accurate for our study. In addition, it is mandatory to analyse which is the reliability of the forecaster when the end user decided to modify the error rate, α after the *M* has been selected. Table 7 shows the calculated error metrics for CL = 90% and CL = 85%, respectively.

Through the analysis of Tables 6 and 7 we conclude that the lower the CL is, the lower the PICP value. This conclusion is supported by the fact that a decrease in the CL is related to a narrower prediction interval, as the results of the WSN, CINAW and SSN error metrics suggested. Therefore, the compromise between the CL and the PICP value is up to the user and will depend on the application and chosen error rate. Figs. 3 and 4 present two examples to show that the actual samples fall into the bounds calculated by the developed CIF (CL = 95%) in the vast majority of the analysed samples. The blue line represents actual temperature measurements and the red lines are the upper and lower bounds computed by our CIF.

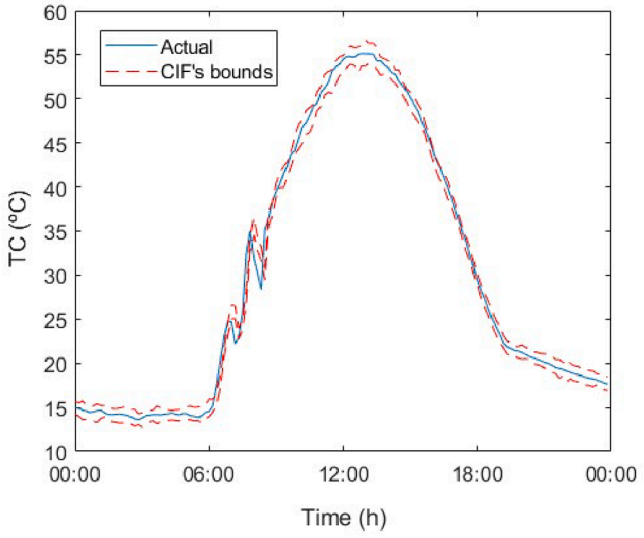

Fig. 5. CIF and actual TC's evolution for August 13, 2017.

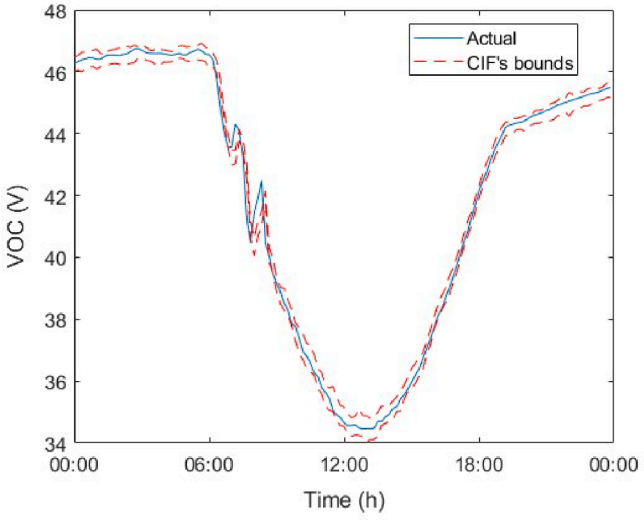

Fig. 6. CIF and actual VOC's evolution for August 13, 2017.

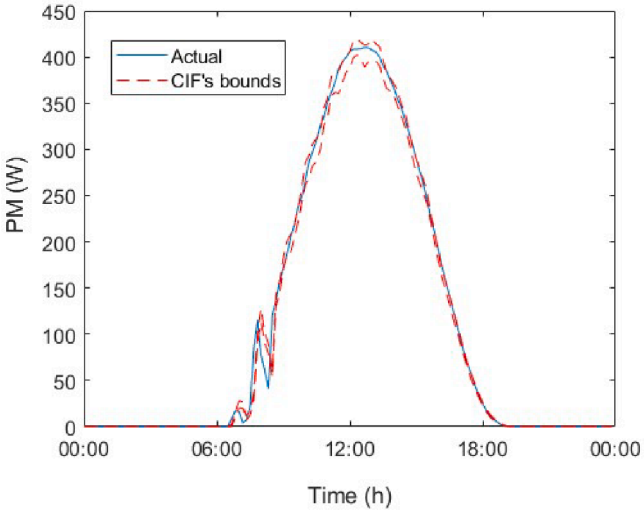

Fig. 7. CIF and PM's evolution for August 13, 2017.

CIF for PV parameters

After concluding that the CIF in the FFNNST model outperforms the reliability as well as the error metric indexes of FFNN's, some simulations were run to examine model's suitability in PV control strategies. Ayvazoğluyüksel et al. [20,55] suggested that key parameters VOC, TC, ISC and PM must be monitored to ensure new reliable control strategies. The TC, VOC and ISC parameters are often used for the assessment of the PV generator's security strategies [20], whereas the PM parameters are required for power management control strategies [17]. TC and VOC are mainly influenced by temperature, whereas ISC is influenced by solar irradiation; PM is influenced by the combination of both [20]. Figs. 5-7 show how developed confidence interval ambient temperature forecaster, combined with Rodríguez et al. [24] proposed solar irradiation forecaster as well as Ayvazoğluyüksel et al. [20] equations allow us to compute TC¸ VOC, PM parameters' bounds for ($CL = 95\%$).

As can be concluded from Figs. 5 to 7, temperature CIFs give relevant information and make it possible to calculate PVs' control parameters such as TC¸ VOC and PM. In the vast majority of cases, and when no sudden solar irradiation changes take place, the actual value falls within the calculated interval. Future research work will focus on calculating a solar irradiation CIF that is able to forecast all relevant control parameters in PV control strategies.

Conclusions

In this study, a parametric ambient temperature confidence interval forecaster was developed. The forecaster predicts the interval for the next 10 min, with a confidence level chosen by the user, and its reliability was checked using the database from Vitoria-Gasteiz, Basque Country. These are the conclusions from this study:

Although all the presented forecasters fulfil the requirement of the PICP being larger than the CL and can be used for temperature forecasting, the final CIF is based on the combination of a FFNNST forecaster and mathematical concepts where PDFs are taken into account.

The CIF's accuracy was analysed for different CLs: 95%, 90% and 85%. As expected, the lower the confidence level is, the lower CIF accuracy is. However, the sharpness or interval width also decreases, which can be convenient depending on the application. Therefore, the user should choose whether higher reliability or a narrower interval is desirable.

All the numerical results presented in this study and the sensitivity analyses were run with data from Vitoria-Gasteiz, Basque Country. Although the proposed methodology for CIF can be easily applied in other locations, one of the main disadvantages of the present approach is that a database from the target station is needed to fit the parameters of the proposed mathematical model.

Based on the results provided by this study, the ambient temperature CIF can be used to predict the control parameters that are involved in PV generators, such as TC¸ VOC, PM. The CIF provides more information than DPF, so using CIF to assess PV generators' reliability is more convenient for energy management systems.

Declaration of Competing Interest

The authors declare that they have no known competing financial interests or personal relationships that could have appeared to influence the work reported in this paper.

Acknowledgements

The authors would like to thank the Basque Government's Department of Education for financial support through the Researcher Formation Programme; grant number PRE_2019_2_0035. The authors would like to thank Fundación Caja Navarra, Obra Social La Caixa and University of Navarra for financial support through the Mobility Research Formation Programme; grant number MOVIL-2019-25.

References

[1] Rosales-Asensio E, Borge-Diez D, Blanes- Perió JJ, Pérez-Hoyos A, Comenar-Santos A. Review of energy technology and associated market and economic conditions in Spain. Renew Sustain Energy Rev. 2019;101:415–27. https://doi.org/10.1016/j.rser.2018.11.029.

[2] Aguilar-Vargas S, Telles-Estebes GR, Medina-Maçaira P, Bastos Q, Cyrino-Oliveira FL, Castro-Souza R. Wind power generation: A review and a research agenda. J Clean Prod. 2019;218:850–70. https://doi.org/10.1016/j.jclepro.2019.02.015.

[3] REN21, 2014. The first decade: 2004-2014, 10 years of renewable energy progress. http://www.ren21.net/Portals/0/documents/activities/Topical%20Reports/REN21_10yr.pdf (accessed 04/03/2020).

[4] REN21, 2019. RENEWABLES 2019 GLOBAL SATUTS REPORT. https://www.ren21.net/wp-content/uploads/2019/05/gsr_2019_full_report_en.pdf (accessed 04/03/2020).

[5] Sahoo, A.K., Sahoo, S.K., 2016. Energy Forecasting for Grid Connected MW Range Solar PV System. 7th India International Conference on Power Electronics (IICPE). 10.1109/IICPE.2016.8079388.

[6] Rodríguez F, Martín F, Fontán L, Galarza A. Very Short-Term Load Forecaster Based on a Neural Network Technique for Smart Grid Control. Energies. 2020;13(19):5210. https://doi.org/10.3390/en13195210.

[7] Yin L, Yu T, Zhang X, Yang B. Relaxed deep learning for real-time economic generation dispatch and control with unified time scale. Energy. 2018;149:11–23. https://doi.org/10.1016/j.energy.2018.01.165.

[8] Haberg M. Fundamentals and recent developments in stochastic unit commitment. Int J Electr Power Energy Syst. 2019;109:38–48. https://doi.org/10.1016/j.ijepes.2019.01.037.

[9] European Union and International Renewable Energy Agency (IRENA), 2018. Renewable Energy Prospects for the European Union. https://www.irena.org/-/media/Files/IRENA/Agency/Publication/2018/Feb/IRENA_REmap_EU_2018.pdf (accessed 15/03/2020).

[10] International Renewable Energy Agency (IRENA), 2019. https://www.irena.org/-/media/Files/IRENA/Agency/Publication/2019/Feb/IRENA_Innovative_ancillary_services_2019.pdf?la=en&hash=F3D83E86922DEED7AA3DE3091F3E49460C9EC1A0 (accessed 16/03/2020).

[11] Jamal T, Carter C, Schmidt T, Shafiullah GM, Calais M, Urmee T. An energy flow simulation tool for incorporating short-term PV forecasting in a diesel-PV-battery off-grid power supply system. Appl Energy. 2019;254:113718. https://doi.org/10.1016/j.apenergy.2019.113718.

[12] Jahangir H, Golkar MA, Alhameli F, Mazouz A, Ahmadian A, Elkamel A. Short-term wind speed forecasting framework based on stacked denoising auto-encoders with rough ANN. Sustain. Energy Technol. Assess. 2020;38:100601. https://doi.org/10.1016/j.seta.2019.100601.

[13] Li P, Zhou K, Lu X, Yang S. A hybrid deep learning model for short-term PV power forecasting. Appl Energy. 2020;259:114216. https://doi.org/10.1016/j.apenergy.2019.114216.

[14] Ding M, Zhou H, Xie H, Wu M, Nakanishi Y, Yokohama R. A gated recurrent unit neural networks based wind speed error correction model for short-term wind power forecasting. Neurocomputing. 2019;365:54–61. https://doi.org/10.1016/j.neucom.2019.07.058.

[15] Wang S, Wang S, Wang D. Combined probability density model for medium term load forecasting based on quantile regression and kernel density estimation. Energy Proc. 2019;158:6446–51. https://doi.org/10.1016/j.egypro.2019.01.169.

[16] Carvallo JP, Larsen PH, Sanstad AH, Goldman CA. Long term load forecasting accuracy in electric utility integrated resource planning. Energy Policy. 2018;119:410–22. https://doi.org/10.1016/j.enpol.2018.04.060.

[17] Elsinga B, van Sark WGJHM. Short-term peer-to-peer solar forecasting in a network of photovoltaic systems. Appl Energy. 2017;206:1464–83. https://doi.org/10.1016/j.apenergy.2017.09.115.

[18] Lorenz E, Heineman D. Prediction of Solar Irradiance and Photovoltaic Power. Compreh Renew Energy. 2012;1:239–92. https://doi.org/10.1016/B978-0-08-087872-0.00114-1.

[19] Diagne M, David M, Lauret P, Boland J, Schmutz N. Review of solar irradiance forecasting methods and a proposition for small-scale insular grids. Renew Sustain Energy Rev. 2013;27:65–76. https://doi.org/10.1016/j.rser.2013.06.042.

[20] Ayvazoğluyüksel Ö, Filik ÜB. Estimation methods of global solar irradiation, cell temperature and solar power forecasting: A review and a case study in Eskişehir. Renew Sustain Energy Rev. 2018;91:639–53. https://doi.org/10.1016/j.rser.2018.03.084.

[21] Mattei M, Notton G, Cristofari C, Muselli M, Poggi P. Calculation of the polycrystalline PV module temperature using a simple method of energy balance. Renew Energy. 2006;31(4):553–67. https://doi.org/10.1016/j.renene.2005.03.010.

[22] Skoplaki E, Boudouvis AG, Palyvos JA. A simple correlation for the operating temperature of photovoltaic modules of arbitrary mounting. Sol Energy Mater Sol Cells. 2008;92(11):1393–402. https://doi.org/10.1016/j.solmat.2008.05.016.

[23] Schwingshackl C, Petitta M, Wagner JE, Belluardo G, Moser D, Castelli M, et al. Wind effect on PV module temperature analysis of different techniques for an accurate estimation. Energy Procedia 2013;40:77–86. https://doi.org/10.1016/j.egypro.2013.08.010.

[24] Rodríguez F, Martín F, Fontán L, Galarza A. Ensemble of machine learning and spatiotemporal parameters to forecast very short-term solar irradiation to compute photovoltaic generators' output power. Energy. 2021;229:120647. https://doi.org/10.1016/j.energy.2021.120647.
[25] Bouzgou H, Gueymard CA. Fast short-term global solar irradiance forecasting with wrapper mutual information. Renew Energy. 2019;133:1055–65. https://doi.org/10.1016/j.renene.2018.10.096.
[26] Liu Z, Jiang P, Zhang L, Niu X. A combined forecasting model for time series: Application to short-term wind speed forecasting. Appl Energy. 2020;259:114137. https://doi.org/10.1016/j.apenergy.2019.114137.
[27] Duan Z, Liu H. An evolution-dependent multi-objective ensemble model of vanishing moment with adversarial auto-encoder for short-term wind speed forecasting in Xinjiang windfarm. China. Energy Conv Manag. 2019;198:111914. https://doi.org/10.1016/j.enconman.2019.111914.
[28] Zhang X, Tan SC, Li G. Development of an ambient air temperature prediction model. Energy Build. 2014;73:166–70. https://doi.org/10.1016/j.enbuild.2014.01.006.
[29] Papantoniou S, Kolokotsa DD. Prediction of outdoor air temperature using neural networks: Application in 4 European cities. Energy Build. 2016;114:72–9. https://doi.org/10.1016/j.enbuild.2015.06.054.
[30] Rodríguez F, Florez-Tapia AM, Fontán L, Galarza A. Very short-term wind power density forecasting trough artificial neural networks for microgrid control. Renew Energy. 2020;145:1517–27. https://doi.org/10.1016/j.renene.2019.07.067.
[31] Bakker K, Whan K, Knap W, Schmeits M. Comparison of statistical post-processing methods for probabilistic NWP forecast of solar irradiation. Sol Energy. 2019;191:138–50. https://doi.org/10.1016/j.solener.2019.08.044.
[32] Caldas M, Alonso-Suárez R. Very short-term solar irradiance forecast using all-sky imaging and real time measurements. Renew Energy. 2019;143:1643–58. https://doi.org/10.1016/j.renene.2019.05.069.
[33] Sivaneasan B, Yu CY, Goh KP. Solar Forecasting uing ANN with Fuzzy Logic Pre-processing. Energy Proc. 2017;143:727–32. https://doi.org/10.1016/j.egypro.2017.12.753.
[34] Jiang H, Dong Y. A nonlinear support vector machine model with hard plenty function based on glowworm swarm optimization for forecasting daily global solar radiation. Energy Conv Manag. 2016;126:991–1002. https://doi.org/10.1016/j.enconman.2016.08.069.
[35] Huang J, Korolkiewicz M, Agrawal M, Boland J. Forecasting solar radiation on an hourly time scale using Coupled AutoRegressive and Dynamical System (CARDS) model. Sol Energy. 2013;83:342–9. https://doi.org/10.1016/j.solener.2012.10.012.
[36] Kushwaha V, Pindoriya NM. A SARIMA-RVFL hybrid model assisted by wavelet decomposition for very-short term solar PV power generation forecast. Renew Energy. 2019;140:124–39. https://doi.org/10.1016/j.renene.2019.03.020.
[37] Li K, Wang R, Lei H, Zhang T, Liu Y, Zheng X. Interval prediction of solar power using an improved bootstrap method. Sol Energy. 2018;159:97–112. https://doi.org/10.1016/j.solener.2017.10.051.
[38] Liu L, Zhao Yi, Chang D, Xie J, Ma Z, Sun Q, et al. Prediction of short-term PV power output and uncertainty analysis. Appl Energy. 2018;228:700–11. https://doi.org/10.1016/j.apenergy.2018.06.112.
[39] Yan X, Abbes D, Francios B. Uncertainty analysis for day ahead power reserve quantification in an urban microgrid including PV generators. Renew Energy. 2017;106:288–97. https://doi.org/10.1016/j.renene.2017.01.022.
[40] Zhang, J., Yan, J., Infield, D., Liu, Y., Lien, F., 2019. Short-term forecasting and uncertainty analysis of wind turbine power based on log sort-term memory network and Gaussian mixture model. 241. 229-244. 10.1016/j.apenergy.2019.03.044.
[41] Fonseca Junior JGdS, Oozeki T, Ohtake H, Takashima T, Kazuhiko O. On the Use of Maximum Likelihood and Input Data Similarity to Obtain Prediction Intervals for Forecasts of Photovoltaic Power Generation. J Electr Eng Technol. 2015;10(3):1342–8. https://doi.org/10.5370/JEET.2015.10.3.1342.
[42] Golestaneh F, Pinson P, Gooi HB. Very short-term nonparametric probabilistic forecasting for renewable energy generation – With application to solar energy. IEEE Trans Power Syst. 2016;31:3850–63. https://doi.org/10.1109/TPWRS.2015.2502423.
[43] Gallego-Castillo C, Bessa R, Cavalante L, Lopez-Garcia O. On-line quantile regression in the RKHS (Reproducing Kernel Hilbert Space) for operational probabilistic forecasting of wind power. Energy. 2016;113:355–65. https://doi.org/10.1016/j.energy.2016.07.055.
[44] Khosravi F, Izbirak G, Shavarani SM. Application of bootstrap re-sampling method in statistical measurement of sustainability. Socio-Econ. Plan. Sci. 2021;75:100781. https://doi.org/10.1016/j.seps.2020.100781.
[45] Rodríguez F, Genn M, Fontán L, Galarza A. Very short-term temperature forecaster using MLP and N-nearest stations for calculating key control parameters in solar photovoltaic generation. Sustainable Energy Technol Assess 2021;45:101085. https://doi.org/10.1016/j.seta.2021.101085.
[46] Marquardt DW. An Algorithm for Least-Squares Estimation of Nonlinear Parameters. SIAM J. Appl. Math. 1963;11(2):431–41. https://doi.org/10.1137/0111030.
[47] Seber, G.A., Wild, C.J., 1989. Nonlinear Regression. John Wiley & Sons, Inc. New York. 10.1002/0471725315.
[48] Golestaneh F, Pinson P, Gooi HB. Very Short-Term Nonparametric Probabilistic Forecasting of Renewable Energy Generation – With Application to Solar Energy. IEEE Trans. Power Syst. 2016;31(5):3850–63. https://doi.org/10.1109/TPWRS.2015.2502423.
[49] Winkler RL. A decision-theoretic approach to interval estimation. J Am Stat Assoc. 1972;67(337):187–91.
[50] Liu Y, Qin H, Zhang Z, Pei S, Wang C, Yu X, et al. Ensemble spatiotemporal forecasting of solar irradiation using variational Bayesian convolutional gate recurrent gate recurrent unit network. Appl Energy. 2019;253:113596. https://doi.org/10.1016/j.apenergy.2019.113596.
[51] Pereira S, Canhoto P, Salgado R, Costa MJ. Development of ANN based corrective algorithm of the operational ECMWF global horizontal irradiation forecast. Sol Energy. 2019;185:387–405. https://doi.org/10.1016/j.solener.2019.04.070.
[52] Majumder I, Dash PK, Bisoi R. Variational mode decomposition based low rank robust kernel extreme learning machine for solar irradiation forecasting. Energy Conv Manag. 2018;171:787–806. https://doi.org/10.1016/j.enconman.2018.06.021.
[53] Heydari A, Astiaso Garcia D, Keynia F, Bisegna F, De Santoli L. A novel composite neural network based method for wind and solar power forecasting in microgrids. Appl Energy. 2019;251:113353. https://doi.org/10.1016/j.apenergy.2019.113353.
[54] Ouyang T, Zha T, Qin L. A combined multivariate model for wind power prediction. Energy Conv Manag. 2017;144:361–73. https://doi.org/10.1016/j.enconman.2017.04.077.
[55] Pachal G, Ganatra A, Kosta YP, Panchal D. Behaviour analysis of multilayer perceptrons with multiple hidden neurons and hidden layers. Int J Comp T Eng. 2011;3:332–7. https://doi.org/10.7763/IJCTE.2011.V3.328.